

# The Impact of a Buried High-Velocity Layer in the Seismic Site Amplification of the City of Llole, Chile

by Miguel Sáez, César Pastén, Sergio Ruiz, and José Salomón

**Abstract** We studied the influence of a buried high-velocity layer (HVL) on the surface ground amplification of the city of Llole, Chile, where large peak ground accelerations were observed during the 1985  $M_w$  8.0 Valparaíso and the 2010  $M_w$  8.8 Maule earthquakes. This study compares the theoretical and empirical surface response of a borehole seismic array located over a 60-m depth soil deposit consisting of sandy and clayey soil layers with shear-wave velocities ( $V_S$ ) ranging from 200 to 720 m/s down to the bedrock and a 5-m-thick gravelly HVL at 21-m depth. The seismic array is composed of accelerometers at the surface, the middle, and the bottom of the soil deposit, which allowed us to estimate the 1D empirical transfer function by computing spectral ratios from 16 earthquakes with magnitudes  $4.2 < M_w < 6.0$ . The empirical spectral ratios between the surface and the bedrock show a complex seismic behavior characterized by four resonance frequencies with similar amplitudes between 2 and 10 Hz. We compared the empirical results with standard theoretical and experimental methods used in site characterization and found that the presence of the HVL in the city of Llole introduces complexities in the seismic behavior of the site that cannot be captured by individual standard methods.

*Electronic Supplement:* Description of the procedure implemented to calculate the empirical dispersion curves reported in the main article and tables of the earthquakes recorded by the seismic array used to calculate the empirical spectral ratios.

## Introduction

The shear-wave velocity ( $V_S$ ) profile and the thickness of the soil layers are two of the most important parameters that determine the seismic site response (Steidl *et al.*, 1996). These properties control the frequency content, the duration, and the intensity of the surface ground motion during earthquakes (Borcherdt, 1970). Nowadays, surface-wave methods (SWMs) have been preferred in the estimation of  $V_S$  profiles because of their simpler implementation, low cost, and depth of investigation compared with traditional invasive techniques (Foti *et al.*, 2011). Despite the several advantages, the use of SWMs to study complex profiles that include a high-velocity layer (HVL) is limited by the insensitivity of the phase-velocity dispersion curve to the  $V_S$  of such layer (Shen *et al.*, 2016) and by the nonuniqueness of the inverse problem (Luke and Calderón-Macías, 2007; Foti *et al.*, 2009; Farrugia *et al.*, 2017). To overcome these limitations, advanced inversion algorithms have been proposed to detect thin shallow HVLS (Luke and Calderón-Macías, 2007) and combined SWMs to detect low-velocity layers (LVLs; Farrugia *et al.*, 2016). In general, most studies focus on detecting the properties of these irregular layers ( $V_S$  and thickness of HVL and LVL) and obtaining robust  $V_S$  profiles

using invasive or noninvasive methods. However, the influence of the HVL on the surface response has scarcely been reported (Farrugia *et al.*, 2016) because of the costs of obtaining a reliable empirical transfer function for the site with respect to either a nearby outcrop or the underlying bedrock.

In central Chile, the 1985  $M_w$  8.0 Valparaíso and the 2010  $M_w$  8.8 Maule megathrust earthquakes struck the city of Llole (epicenters of the earthquakes are shown in Fig. 1a), resulting in large peak ground accelerations (PGAs) in the LLO seismic station (Fig. 1b; Ruiz *et al.*, 2012). Despite the different seismic sources of both earthquakes, the Fourier spectra (FS) of the east–west (E–W in Fig. 2a), north–south (N–S in Fig. 2b), and vertical (Z in Fig. 2c) components of motion are similar in a wide range of frequencies, which hints at the soil deposit as one of the factors for the akin seismic behavior of the site. Because of the high PGAs recorded during the 1985 Valparaíso earthquake ( $PGA_Z = 0.81g$ ,  $PGA_{E-W} = 0.65g$ ,  $PGA_{N-S} = 0.41g$ ), the first Chilean borehole seismic array composed of three accelerometers and two piezometers was deployed at 1.0 km from the LLO station (Fig. 1b). The 60-m-depth soil deposit where

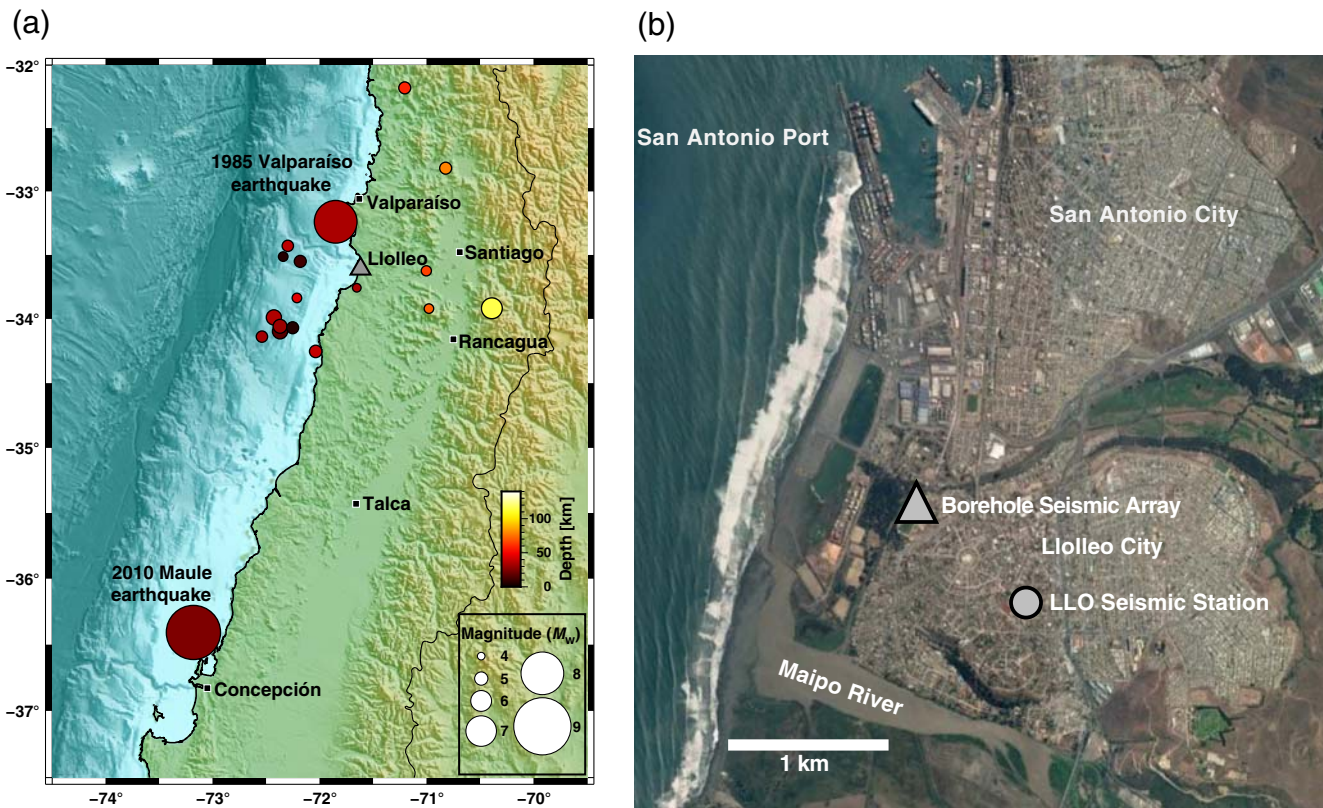


**Figure 1.** City of Lloleco and the study area. (a) Epicenters of seismic events (circles) used for the calculation of the empirical spectral ratios (ESRs) along with the 1985 Valparaíso and the 2010 Maule earthquakes; (b) location of the borehole seismic array and the LLO seismic station. The color version of this figure is available only in the electronic edition.

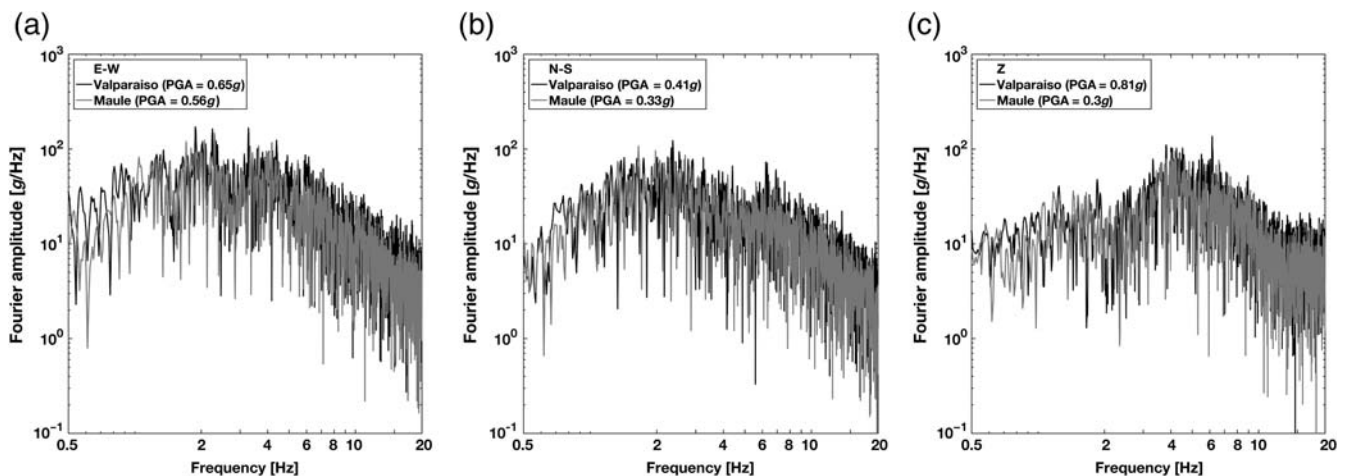


**Figure 2.** Fourier spectra (FS) of the (a) east–west (E-W), (b) north–south (N-S), and (c) vertical (Z) components records of the 1985 Valparaíso and the 2010 Maule earthquakes, respectively.

the array was installed consists of sandy, clayey, and gravelly soil layers that were investigated with traditional geotechnical tests, a crosshole test down to 20-m depth, and a down-hole test down to the bedrock to determine the  $P$ - and  $S$ -wave velocity profiles (Verdugo, 2009). The main characteristic of the soil deposit is the presence of a 5-m-thick high-velocity gravel layer at 21-m depth (Fig. 3a).

Unlike most studies that focus on the comparison of the soil profile obtained with invasive and noninvasive methods (Xia *et al.*, 2002) and on the capabilities of different techniques to detect an HVL (Jin and Luke, 2006; Luke and Calderón-Macías, 2007; Murvosh *et al.*, 2013), this study attempts to explain the role that a HVL plays in the seismic site response of a soil deposit with the presence of such layer

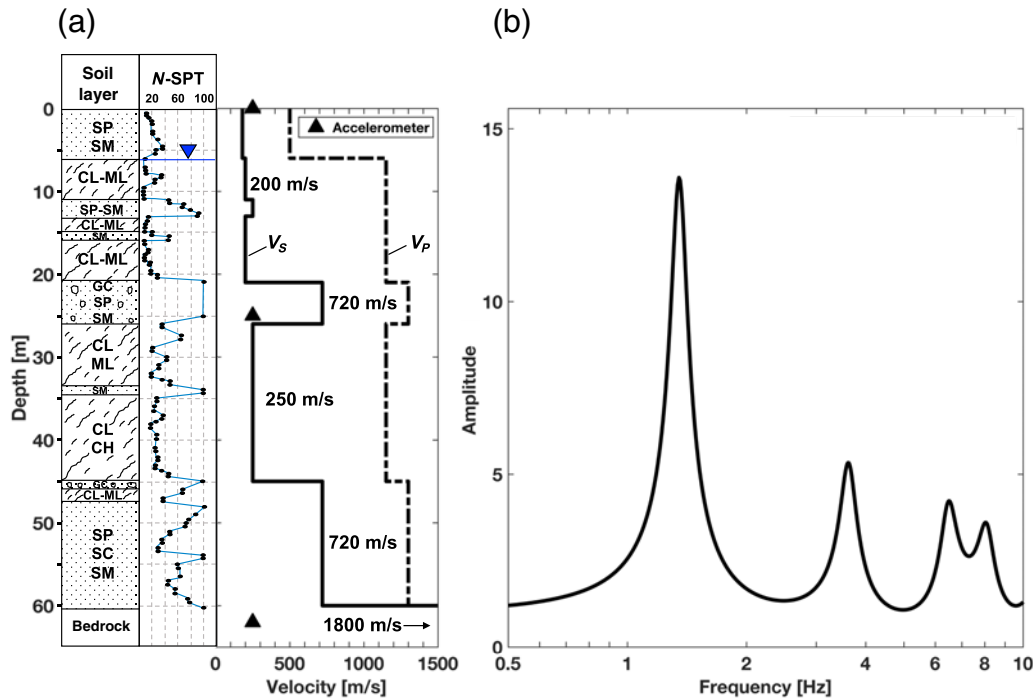


**Figure 3.** The borehole seismic array: (a) geotechnical soil classification, blow count per foot from the standard penetration test ( $N$ -SPT),  $P$ - and  $S$ -wave velocity profiles from downhole and crosshole tests (Verdugo, 2009). Triangles show the location of the triaxial accelerometers in the soil profile. (b) Theoretical  $SH$ -wave transfer function of the soil profile with constant material properties. The color version of this figure is available only in the electronic edition.

and the capabilities of standard methodologies to predict the soil seismic behavior. We computed the theoretical  $SH$ -wave transfer function and the theoretical phase-velocity dispersion curve from results of crosshole and downhole tests and empirical spectral ratios (ESRs) from earthquake records, as well as horizontal-to-vertical (H/V) spectral ratios (HVSRS) and phase-velocity dispersion curves from ambient seismic noise measurements. Based on these results, we discuss the influence of the HVL on the seismic behavior of the city of Llole.

### The Llole Borehole Seismic Array

The borehole seismic array, located at the west of the city of Llole (Fig. 1b), consists of three force balance triaxial accelerometers SSA-320SS installed at the ground surface and inside two boreholes at 24- and 62-m depth (Fig. 3a). The trigger level of the accelerometers was set to  $0.001g$  at a sampling rate of 50 samples per second. The seismic array operated for 6 yrs from 1998 and recorded the N-S, E-W, and Z components of 16 earthquakes with moment magnitudes between  $M_w$  4.2 and 6.0 (Verdugo, 2009). The epicenters of the earthquakes are shown in Figure 1a, and their main characteristics are listed in Table S1 (available in the electronic supplement to this article). The distribution of earthquake epicenters is not uniform around the station, lacking earthquakes from the southeast and the northwest directions.

Geotechnical characterization tests performed at the site shows that the soil profile is composed of clayey, sandy, and gravelly soil layers. Standard penetration test blow counts ( $N$ -SPT) exhibit high variability with depth and layers with high penetration resistance (Fig. 3a). The  $V_S$  profile obtained from downhole and crosshole tests shows a shallower 21-m-thick sand and clay interbedded layers with average shear-wave velocities of 200 m/s, a 5-m-thick stiff gravel layer with a high shear-wave velocity of 720 m/s, a 19-m-thick clayey layer with a shear-wave velocity of 250 m/s, and finally a 15-m-thick stiff sandy layer with a shear-wave velocity of 720 m/s over the bedrock, whose  $V_S$  was estimated at around 1800 m/s (Verdugo, 2009).

### Theoretical $SH$ -Wave Transfer Function

Multilayer  $V_S$  and  $V_P$  profiles obtained from the crosshole and downhole tests were used to calculate the theoretical transfer function of the soil deposit with respect to the underlying bedrock, assuming a vertically incident shear-wave ( $SH$ -wave transfer function) and using the solution of the wave-propagation equation for viscoelastic materials. The theoretical  $SH$ -wave transfer function was calculated between 0.5 and 10 Hz (Fig. 3b) with constant material damping and stiffness (i.e., without stiffness degradation). In addition, we calculated transfer functions considering nonlinear soil behavior using the equivalent-linear software EERA (Bardet *et al.*, 2000) and the 16 analyzed earthquake records in the bedrock as input motions (Fig. 4). The input

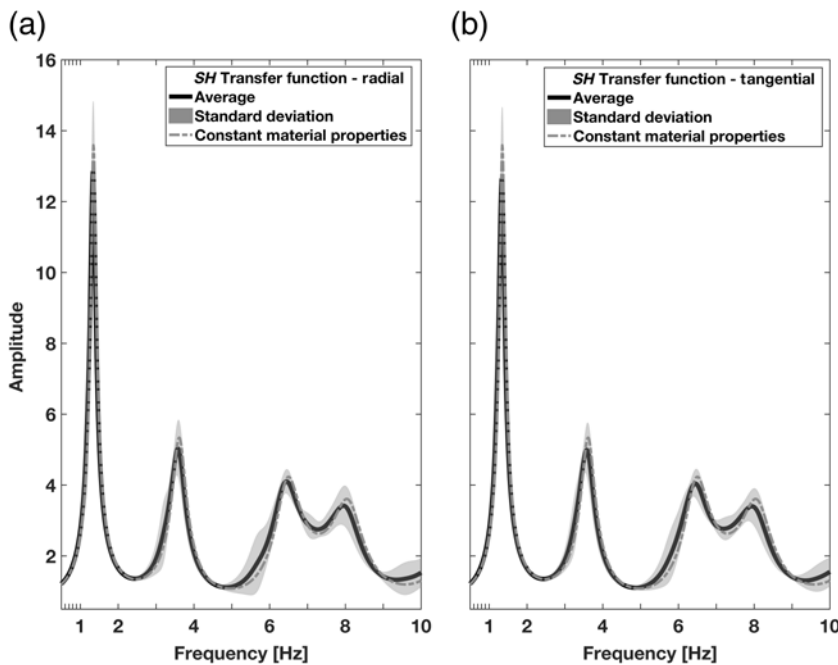


**Figure 4.** Average transfer functions between the surface and the base of the soil deposit obtained with the EERA software in the (a) radial and (b) tangential directions of the 16 analyzed earthquakes.

seismic records were rotated to radial and tangential components depending on the azimuth between the seismic array and the earthquake source. Material stiffness degradation curves ( $G/G_{\max}$ ; Seed and Iris, 1970; Schnabel *et al.*, 1972; Seed *et al.*, 1986; Sun *et al.*, 1988) and damping ratios considered in this analysis are detailed in Table S2 and Figure S1. In both analyses, the soil densities used in the calculation of the transfer functions were assumed as a function of the  $V_S$  according to Cadet *et al.* (2012), and the damping ratio was set to 5% for the soil and 2% for the bedrock (Oztoprak and Bolton, 2013). The theoretical  $SH$ -wave transfer function with constant material properties shows the fundamental frequency at 1.35 Hz and the next resonance frequencies at 3.61, 6.47, and 8.07 Hz (Fig. 3b). On the other hand, the average equivalent-linear transfer function shows resonance frequencies at 1.34, 3.58, 6.45, and 7.95 Hz (Fig. 4). The similarity between the resonance frequencies obtained from the equivalent-linear method and the solution with constant material properties suggests that the analyzed earthquakes did not cause a pronounced nonlinear behavior. For this reason, we will consider only the theoretical transfer function with constant material properties in what follows.

#### Empirical Spectral Ratios of Earthquakes Records

The strong motions recorded by the borehole seismic array were used to calculate ESRs for tangential and radial components as estimates of the soil deposit transfer function.

We followed the methodology described by Ghofrani *et al.* (2013) that implements the next steps:

1. rotate the N-S and the E-W components of a seismic record according to the azimuth between the seismic array and the earthquake source to obtain the radial and tangential components;
2. compute the FS of the radial and the tangential components and smooth each one with a Konno–Ohmachi’s filter using a bandwidth coefficient  $b = 40$  (Konno and Ohmachi, 1998);
3. resample the smoothed FS using a logarithmic sequence of 100 points between 0.1 and 10 Hz;
4. calculate the ESR as the ratio between the smoothed FS of the record at the surface and the smoothed FS of the record at the soil deposit base in the radial and tangential components; and
5. calculate the average ESR as the geometric average between the ESRs in the radial and the tangential components.

We did not further correct the spectral ratios by empirical correction factors as Ghofrani *et al.* (2013) recommended and did not apply destructive interference correction because the available records were not perfectly synchronous to calculate the correlation between the surface and the downhole records (Steidl *et al.*, 1996).

The average spectral ratios between the surface and the base in the tangential and the radial directions show four clear peaks for the 16 analyzed earthquakes (see Fig. 5a and 5b, respectively). Whereas the tangential spectral ratio has resonance frequencies at 2.0, 4.1, 7.3, and 9.3 Hz, the radial spectral ratio has resonance frequencies at 2.1, 4.3, 7.4, and 9.2 Hz. The amplitude of the spectral ratios exceeds 7 at frequencies higher than 1.5 Hz. Furthermore, the average FS of the 16 analyzed earthquakes in the E-W and N-S components at the surface show three main peaks and a broadband peak in the vertical component with maximum amplitude at 5.4 Hz (Fig. 6). Whereas the average E-W spectrum has the main peak amplitudes at 1.9, 4.3, and 7.1 Hz and a minor peak at 8.9 Hz, the average N-S spectrum has the main peak amplitudes at 2.2, 4.1, and 7 Hz and three minor peaks at 1.7, 5.7, and 8.7 Hz.

#### Passive Seismic Arrays

Different passive seismic arrays were deployed using three-component Tromino sensors to calculate average FS (E-W, N-S, and vertical components) and HVSRs from ambient seismic noise records, as well as a representative velocity dispersion curve for the site. Six different configurations were arranged next to the borehole seismic array with four to

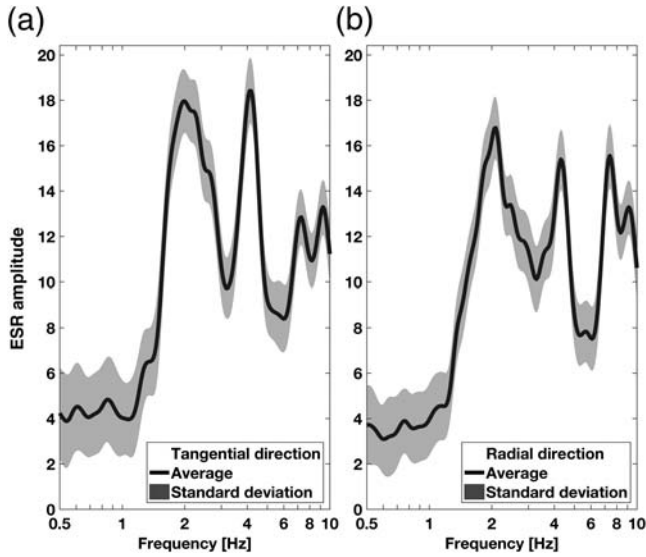


**Figure 5.** Average ESRs between the surface and the base of the soil deposit in the (a) tangential and (b) radial directions from the 16 analyzed earthquakes. The shaded area indicates the associated standard deviation.

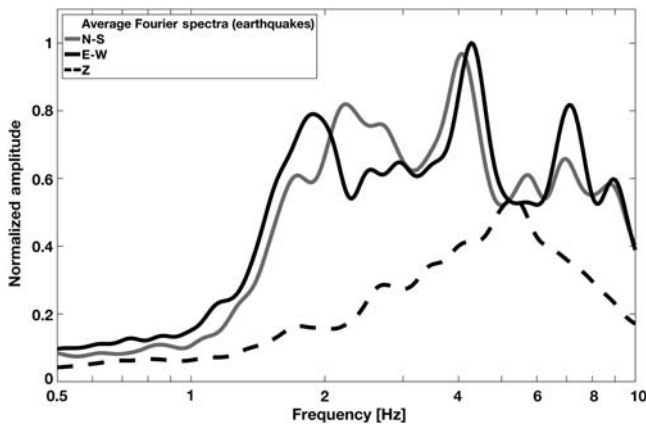


**Figure 6.** Average FS of the surface records in the N-S (gray line), E-W (solid black line), and vertical (dashed black line) directions from the 16 analyzed earthquakes.

seven sensors in each experiment. The intersensor distances ranged between 8 and 150 m, with recording times varying between 20 and 40 min (Fig. 7a).

The average ambient noise FS obtained from the stations closer to the borehole array in Figure 7b were calculated between 0.2 and 10 Hz using the Geopsy software. The ambient noise records were divided into 25-s windows, and the ratio between the short-term average (STA) over a 1-s window and the long-term average (LTA) over a 25-s window were calculated to remove transient noise. Only windows with STA/LTA ratios between 0.2 and 2.5 were considered to calculate the average spectra. In each window that satisfies the criterion, the FS was calculated and smoothed with a Konno–Ohmachi filter using a bandwidth coefficient

$b = 40$  (Konno and Ohmachi, 1998). The final average spectrum in each component was calculated as the average of the 92 available windows (Fig. 7b). In addition, the ambient seismic noise HVSRs were calculated between 0.2 and 10 Hz by dividing the geometric average of the horizontal spectra by the average vertical spectrum in every window (Fig. 8a).

The average ambient noise FS have multiple peak frequencies in the E-W and the N-S components, and the vertical component shows broadband amplitude that peaks at 5.5 Hz (Fig. 7b). The average E-W spectrum has peak frequencies at 2.4 and 4.1 Hz, and the N-S component has peak frequencies at 2.2 and 4.1 Hz. It is worth noting that the horizontal amplitudes are higher than the vertical amplitude below 4.7 Hz, but they are lower than the vertical amplitude at higher frequencies, which hinders the peaks in the spectral ratios at high frequencies (Fig. 8a). The HVSRs results indicate that the average predominant frequency of the site is around 1.92 Hz (Fig. 8a). The large peak amplitude is consistent with the high impedance contrast between the soil deposit and the bedrock displayed in Figure 3a.

An experimental phase-velocity dispersion curve was calculated using the cross correlation between simultaneous ambient noise records from each array shown in Figure 7a. Aki (1957) proposed that the real part of the cross-correlation spectrum between two simultaneous signals approximates a zero-order Bessel function of the first kind. Thus, associating the zero crossings of the real part of the cross spectrum with the zeros of the zero-order Bessel function of the first kind  $J_0$  and considering a constant distance between the sensors, it is possible to estimate the phase velocity of the medium between the sensors (Ekström *et al.*, 2009). We calculated a phase-velocity dispersion curve for each available station pair following the spectral methodology proposed by Pastén *et al.* (2016), dividing the records in 10-s windows (see the electronic supplement for further details). The dispersion curves were resampled between 2 and 30 Hz using a 50-point logarithmic scale, and the average phase velocity and its standard deviation were calculated for every frequency. The average dispersion curve in Figure 8b shows phase velocities decreasing from 600 m/s at 2 Hz to 180 m/s at 30 Hz. The spectral methodology allows calculating the phase velocities for the longest wavelength  $\lambda_{\max} = r_{\max}/0.38$ , in which  $r_{\max}$  is the maximum interstation distance (Calkins *et al.*, 2011). In this study,  $\lambda_{\max} = 150 \text{ m}/0.38 \approx 395 \text{ m}$  (see the geometrical configuration of the sensors in Fig. 7a), which is associated with a frequency of 2 Hz. The maximum frequency of 30 Hz allows capturing wavelengths shorter than 6 m. The lack of resolution at frequencies lower than the HVSR peak frequency may be explained because the soil deposit can create a high-pass filter with a corner frequency near the predominant soil frequency (Scherbaum *et al.*, 2003). The dispersion curve does not show the superposition of higher modes that usually exhibit these types of profiles (Arai and Tokimatsu, 2005) because the spectral methodology used herein assumes that the cross correlation of seismic noise

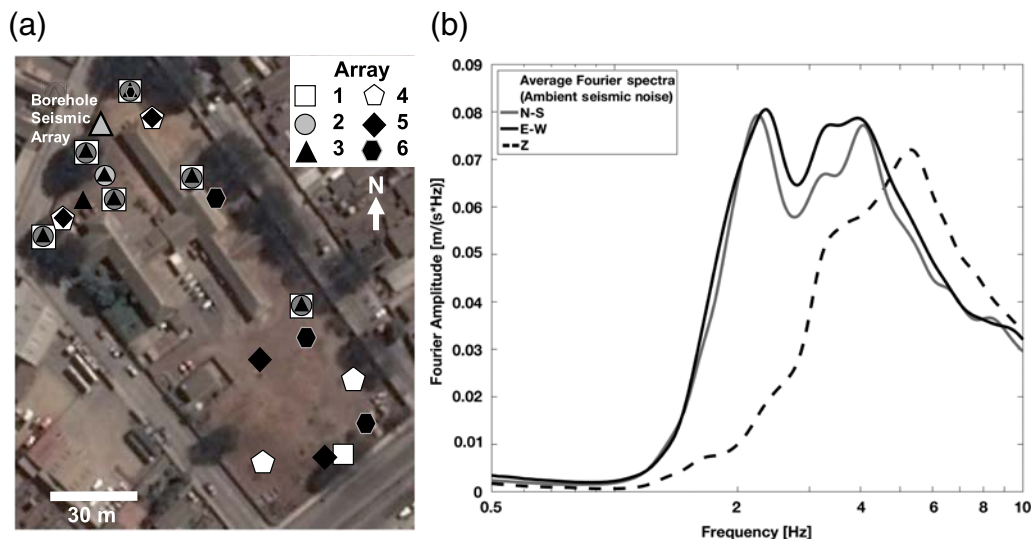


**Figure 7.** Spectral response from the ambient seismic noise records. (a) Location of the Tromino sensors in each of the six deployed arrays; (b) average FS of the records in N-S, E-W, and vertical directions. The color version of this figure is available only in the electronic edition.

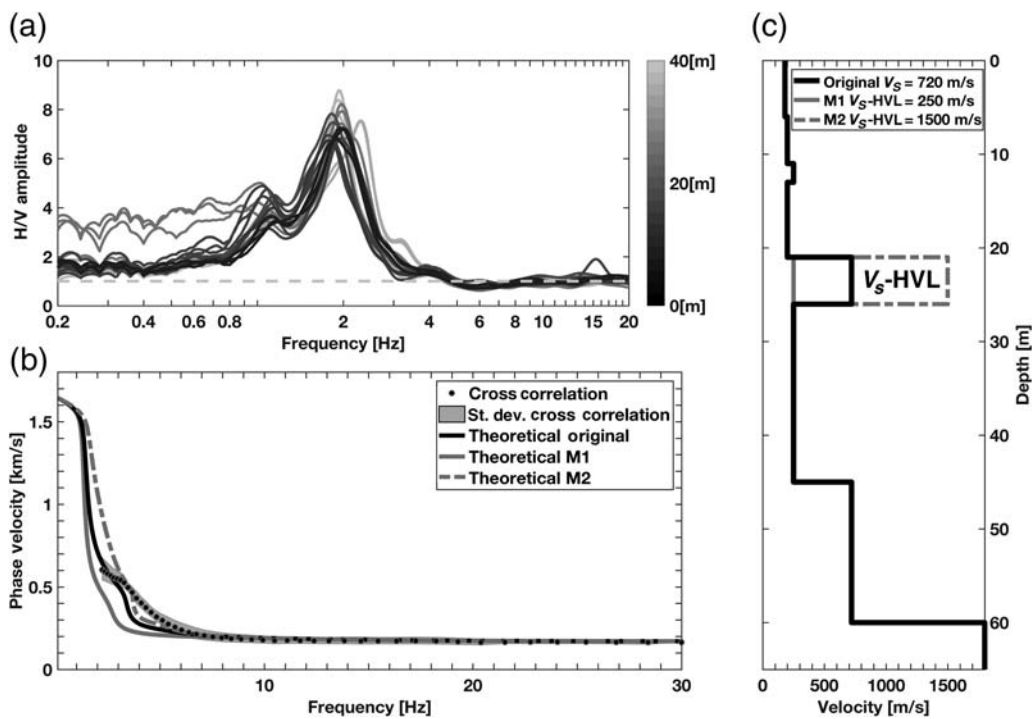


**Figure 8.** Horizontal-to-vertical spectral ratio (HVSr) and dispersion curves from ambient seismic noise records. (a) HVSr obtained from 19 stations located at distances closer than 40 m from the seismic array (the grayscale is proportional to the distance). (b) Phase velocities obtained from the passive seismic arrays compared to the theoretical dispersion curves of the profiles shown in (c). (c) Profiles with different  $S$ -wave velocities for the high-velocity layer (HVL; M1 and M2).

is dominated by the fundamental mode (Ekström, 2014). Furthermore, the average of the experimental phase-velocity dispersion curve and its associated standard deviation were inverted through a neighborhood algorithm (Wathelet *et al.*, 2004) using the Dinver package built in the Geopsy software. Dinver has been used in several studies to obtain reliable  $V_S$

profiles (Wathelet, 2008; Garofalo *et al.*, 2016; Leyton *et al.*, 2018; ⑤ see the electronic supplement for further details). The inversion of the experimental phase-velocity dispersion curve indicates that if no borehole data were available, a normal dispersive soil profile can be used to interpret the experimental dispersion curve.

### Comparison between Methods

Table 1 shows the peak and resonance frequencies estimated from the different methods applied in this study. Frequencies from seismic events (ESR and FS) and ambient seismic noise (HVSr, dispersion curves, and FS) methods are larger than those obtained from the theoretical 1D transfer function calculated with data gathered from invasive downhole and crosshole tests. The ESRs and the theoretical *SH*-wave transfer function have four resonance frequencies in the 0.2- and 10-Hz range, but the frequencies do not match. Although the average ESR has a fundamental frequency at 2.07 Hz, the theoretical *SH*-wave transfer function has it at 1.35 Hz (Table 1). In summary, results from empirical methods suggest that the soil profile is stiffer than the prediction of the 1D *SH*-wave propagation theory. The comparison between these curves is pertinent because the analyzed earthquakes have low to intermediate magnitudes that may not strain the soils to nonlinear levels.

The *SH*-wave transfer function is widely used to study site effects (e.g., Chávez-García and Raptakis, 2017). However, this method is insensitive to the presence of a thin buried HVL. We calculated the effect of varying the *S*-wave velocity of the HVL ( $V_S$ -HVL in Fig. 8) on the theoretical *SH*-wave transfer function. Figure 8c shows profiles with three different  $V_S$  for the HVL,  $V_S$ -HVL = 250 m/s (M1 profile),  $V_S$ -HVL = 720 m/s (original profile), and  $V_S$ -HVL = 1500 m/s (M2 profile). Figure 9 shows that a strong increase in the HVL *S*-wave velocity (M2 profile) barely changes the resonance frequencies of the *SH*-wave transfer function, and a decrease in the HVL *S*-wave velocity to a third of the measured value (M1 profile) slightly decreases the fundamental frequency. These results indicate that the inclusion of a relatively thin HVL in a soil profile causes minor changes in the resonance frequencies according to the 1D *SH*-wave propagation theory.

Figure 10 shows that whereas the ESR calculated between the borehole records at the surface and the middle has resonance frequencies at 4.01 and 8.90 Hz, the ESR between the records at the middle and the bedrock has resonance frequencies at 1.88 and 7.19 Hz (Table 1). When these two curves are compared with the ESR between the surface

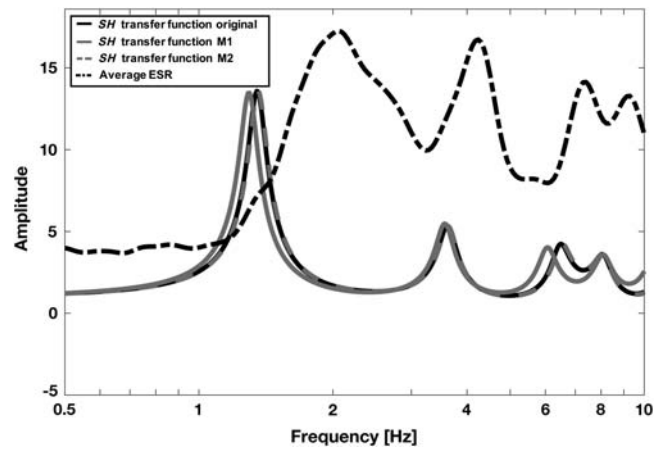


**Figure 9.** Comparison between theoretical *SH*-wave transfer functions of profiles with different *S*-wave velocities for the HVL (Fig. 8c) and the average ESR.

and bedrock, it seems that the latter could be explained as the superposition of two independent systems uncoupled by the HVL. To further explore this feature, we calculated the theoretical *SH*-wave transfer functions between the surface and the bedrock (layer 1/layer 8 in Fig. 11b), the surface and the middle (layer 1/layer 5 in Fig. 11b), and the middle and the bedrock (layer 5/layer 8 in Fig. 11b). The *SH*-wave transfer function between the middle and the bedrock has four resonance frequencies at 1.35, 3.62, 6.42, and 8.1 Hz, respectively (Fig. 11). Furthermore, the *SH*-wave transfer function between the surface and the middle has two resonance frequencies at 2.42 and 6.98 Hz. As observed in the ESR (Fig. 10), the fundamental frequency of the *SH*-wave transfer function middle-bedrock is similar to one of the entire soil profiles and lower than the observed in the *SH*-wave transfer function of the upper 20 m (layer 1/layer 5 in Fig. 11b). However, the 1D theory is not able to reproduce the apparent coupled system observed with the earthquake data. We believe that the phenomenon may be more complex, and future research is needed.

The HVSr technique can be used to estimate the fundamental frequency of a soil deposit and to estimate its transfer function (Ghofrani *et al.*, 2013). However, the HVSr was only able to estimate the fundamental frequency 1.92 Hz at

Table 1  
Comparison between Peak and Resonance Frequencies from Different Methods

Method	$f_1$ (Hz)	$f_2$ (Hz)	$f_3$ (Hz)	$f_4$ (Hz)
Theoretical <i>SH</i> -wave transfer function interpreted from downhole and crosshole tests data with constant material properties (Fig. 3b)	1.35	3.61	6.47	8.07
Average horizontal Fourier spectrum (FS) of seismic events (from E-W and N-S components in Fig. 6)	2.09	4.18	7.03	8.83
Average horizontal FS of ambient seismic noise (from E-W and N-S components in Fig. 7b)	2.31	4.09	—	—
Average horizontal-to-vertical spectral ratio obtained from ambient seismic noise measurements (Fig. 8a)	1.92	—	—	—
Empirical spectral ratio (ESR) between surface and bedrock (ESR surface–bedrock in Fig. 10)	2.07	4.23	7.39	9.26
ESR between surface and middle (ESR surface–middle in Fig. 10)	—	4.01	—	8.90
ESR between middle and bedrock (ESR middle–bedrock in Fig. 10)	1.88	—	7.19	—

E-W, east–west; N-S, north–south.

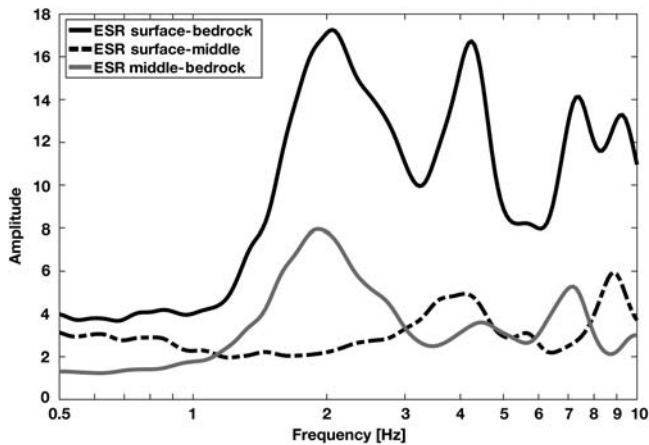


**Figure 10.** Average ESRs between the surface and the bedrock (solid black line), the surface and the middle (dashed black line), and the middle and the bedrock (gray line).

the surface of the seismic borehole array, in contrast to the average FS that also shows the second resonance frequency at 4.09 Hz (Table 1). Although some studies found an excellent correlation between the fundamental frequency of the  $SH$ -wave transfer function and the predominant frequency of the HVSr (Oubaiche *et al.*, 2016), the case of the city of Llole suggests that this relationship is not valid in the presence of an HVL.

Although the frequency range of the measured dispersion curve (from 2 to 30 Hz in Fig. 8b) would allow defining the velocity profile of the soil deposit from the surface to the bedrock (Renalier *et al.*, 2010), the influence of a thin HVL in the dispersion curve is not easily detectable

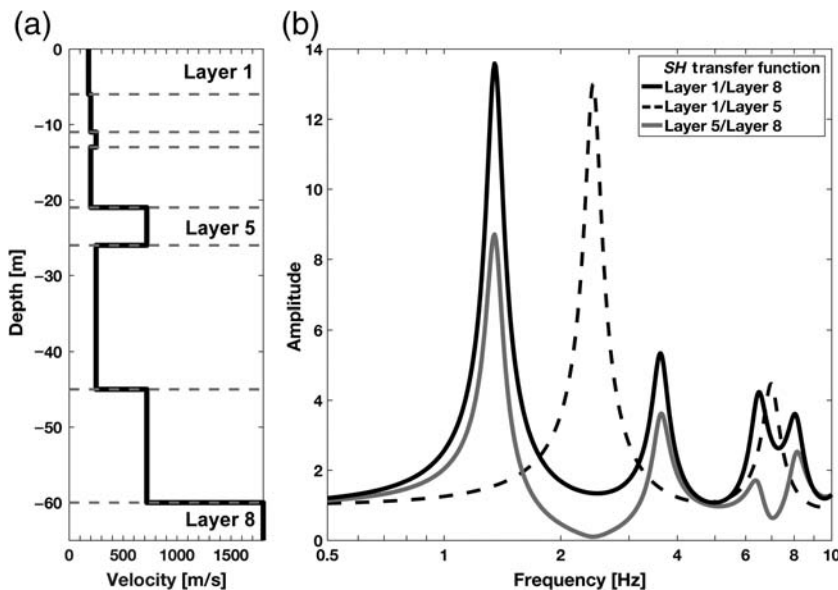


**Figure 11.** Theoretical transfer functions between different layers of the soil profile. (a)  $S$ -wave velocity profile from Figure 3a. (b) Theoretical  $SH$ -wave transfer functions between the surface and the bedrock (layer 1/layer 8), the surface and the middle (layer 1/layer 5), and the middle and the bedrock (layer 5/layer 8).

because of the insensitivity of the dispersion curve to variations in the shear-wave velocity of the HVL (Shen *et al.*, 2016). Figure 8b shows that the theoretical dispersion curve of the profile with a thin HVL of 720 m/s can be regarded as the one of a normally dispersive soil profile. If the HVL shear-wave velocity was increased from 720 to 1500 m/s (M2 profile in Fig. 8b), the variations generated in the dispersion curve are comparable to the errors of the measured dispersion curve.

Unfortunately, we could not implement other methods such as borehole interferometry (Sawazaki *et al.*, 2009; Bonilla *et al.*, 2017) and borehole noise correlation (Zeghal *et al.*, 1995; Rubinstein and Beroza, 2004) because the seismic borehole records were not synchronous, and the sensors were not set to record ambient seismic noise. In addition, we could not perform 1D simulation starting from seismic records at a reference stations because there are not strong ground motion records on outcropping bedrock in the region of interest. The closest station on rock that recorded the 1985 Valparaiso and the 2010 Maule earthquakes was located 60 km north of the LLO station in the city of Valparaiso (Fig. 1a). In the period 1998–2004 when the borehole seismic array operated, no reference station was available near the city of Llole.

## Discussion and Conclusions

We studied the surface ground response of a 60-m depth borehole seismic array located in the city of Llole, where large PGAs were recorded during the 1985 Valparaiso and the 2010 Maule earthquakes. The site is characterized by the presence of a 5-m-thick high-velocity gravel layer at 21-m depth. We implemented a series of standard seismic site characterization methods based on earthquake and ambient noise records.

The average ESR between the surface and the base of the borehole seismic array show four resonance frequencies of similar amplitude between 2 and 10 Hz. This complex behavior is apparently controlled by the HVL and could not be completely predicted by any of the standard methods used in this study.

The theoretical  $SH$ -wave transfer function computed from results of invasive downhole and crosshole tests captures the shape of the ESRs between the bedrock and the surface. However, the theoretical transfer function shows a fundamental frequency near 1.35 Hz that does not agree with the 2.07 Hz obtained from the ESRs.

On the other hand, the HVSr methodology applied to ambient seismic noise is only able to estimate the fundamental frequency of the soil deposit at 1.92 Hz




but not the higher resonance frequencies observed in the ESRs. This limitation is due to high vertical vibration amplitude compared to the horizontal ones at frequencies higher than 4.7 Hz. Given this vertical amplification, we recommend the use of the horizontal motion FS to detect the first two resonance frequencies that are identified in the ESR.

Downhole and crosshole tests are considered two of the most accurate methods for measuring  $V_S$  profiles (Thompson *et al.*, 2009), and theoretical *SH*-wave transfer functions inferred from invasive tests have been used to properly predict empirical transfer functions (Lermo and Chávez-García, 1994; Bonilla *et al.*, 2002). The discrepancy between the theoretical and empirical results in the city of Llole exposes that invasive tests results do not always allow estimating the features of the soil amplification using the 1D *SH*-wave propagation theory in the presence of an HVL.

Because the role of an HVL on the seismic response cannot be correctly characterized with the current state of practice, further research should focus on the numerical simulation of the full wave propagation from the seismic source to the site to elucidate how the surface and body waves interact in the presence of an HVL, as well as on the analysis of borehole seismic arrays with larger databases, including earthquakes with different magnitudes and azimuthal directions.

## Data and Resources

Data from the borehole seismic array are available  in the electronic supplement to this article. The Geopsy software was downloaded from [www.geopsy.org](http://www.geopsy.org) (last accessed February 2018). Details of the Tromino sensors can be found in [www.tromino.eu](http://www.tromino.eu) (last accessed February 2018).

## Acknowledgments

This work was supported by the Programa de Riesgo Sísmico (PRS) at the University of Chile. Miguel Sáez thanks the scholarship PCHA/Doctorado Nacional/2017-21171480, granted by Comisión Nacional de Investigación Científica y Tecnológica (CONICYT). The authors also thank F. Leyton for his helpful advice. Sergio Ruiz thanks the Fondo Nacional de Desarrollo Científico y Tecnológico (FONDECYT) Grant Number 1170430. César Pastén thanks the support from the Advanced Mining Technology Center (AMTC FB0809 PIA CONICYT). The authors thank the anonymous reviewers and the associate editor, who contributed to improve this article.

## References

- Aki, K. (1957). Space and time spectra of stationary stochastic waves, with special reference to microtremors, *Bull. Earthq. Eng.* **35**, 415–456.
- Arai, H., and K. Tokimatsu (2005). *S*-wave velocity profiling by joint inversion of microtremor dispersion curve and horizontal-to-vertical (H/V) spectrum, *Bull. Seismol. Soc. Am.* **95**, no. 5, 1766–1778.
- Bardet, J. P., K. Ichii, and C. H. Lin (2000). *EERA: A Computer Program for Equivalent-Linear Earthquake Site Response Analyses of Layered Soil Deposits*, University of Southern California, Department of Civil Engineering.
- Bonilla, L. F., P. Gueguen, F. Lopez-Caballero, E. D. Mercerat, and C. Gélis (2017). Prediction of non-linear site response using downhole array data and numerical modeling: The Belleplaine (Guadeloupe) case study, *Phys. Chem. Earth* **98**, 107–118.
- Bonilla, L. F., J. H. Steidl, J.-C. Gariel, and R. J. Archuleta (2002). Borehole response studies at the Garner Valley downhole array, southern California, *Bull. Seismol. Soc. Am.* **92**, no. 8, 3165–3179.
- Borcherdt, R. D. (1970). Effects of local geology on ground motion near San Francisco Bay, *Bull. Seismol. Soc. Am.* **60**, no. 1, 29–61.
- Cadet, H., P.-Y. Bard, and A. Rodríguez-Marek (2012). Erratum to: Site effect assessment using KiK-net data: Part 1. A simple correction procedure for surface/downhole spectral ratios, *Bull. Earthq. Eng.* **10**, no. 2, 449.
- Calkins, J. A., G. A. Abers, G. Ekström, K. C. Creager, and S. Rondenay (2011). Shallow structure of the Cascadia subduction zone beneath western Washington from spectral ambient noise correlation, *J. Geophys. Res.* **116**, no. B7, doi: [10.1029/2010JB007657](https://doi.org/10.1029/2010JB007657).
- Chávez-García, F. J., and D. Raptakis (2017). Local amplification and subsoil structure at a difficult site: Understanding site effects from different measurements, *Soil Dynam. Earthq. Eng.* **92**, 334–344.
- Ekström, G. (2014). Love and Rayleigh phase-velocity maps, 5–40 s, of the western and central USA from USArray data, *Earth Planet. Sci. Lett.* **402**, 42–49.
- Ekström, G., G. A. Abers, and S. C. Webb (2009). Determination of surface-wave phase velocities across USArray from noise and Aki's spectral formulation, *Geophys. Res. Lett.* **36**, no. 18, doi: [10.1029/2009GL039131](https://doi.org/10.1029/2009GL039131).
- Farrugia, D., P. Galea, S. D'amico, and E. Paolucci (2017). Sensitivity of ground motion parameters to local shear-wave velocity models: The case of buried low-velocity layers, *Soil Dynam. Earthq. Eng.* **100**, 196–205.
- Farrugia, D., E. Paolucci, S. D'amico, and P. Galea (2016). Inversion of surface-wave data for subsurface shear-wave velocity profiles characterised by a thick buried low-velocity layer, *Geophys. J. Int.* **206**, no. 2, 1221–1231.
- Foti, S., C. Comina, D. Boiero, and L. V. Socco (2009). Non-uniqueness in surface-wave inversion and consequences on seismic site response analyses, *Soil Dynam. Earthq. Eng.* **29**, no. 6, 982–993.
- Foti, S., S. Parolai, D. Albarello, and M. Picozzi (2011). Application of surface-wave methods for seismic site characterization, *Surv. Geophys.* **32**, no. 6, 777–825.
- Garofalo, F., S. Foti, F. Hollender, P. Y. Bard, C. Cornou, B. R. Cox, M. Ohrnberger, D. Sicilia, M. Asten, and G. Di Giulio (2016). InterPA-CIFIC project: Comparison of invasive and non-invasive methods for seismic site characterization. Part I: Intra-comparison of surface wave methods, *Soil Dynam. Earthq. Eng.* **82**, 222–240.
- Ghofrani, H., G. M. Atkinson, and K. Goda (2013). Implications of the 2011 M 9.0 Tohoku Japan earthquake for the treatment of site effects in large earthquakes, *Bull. Earthq. Eng.* **11**, no. 1, 171–203.
- Jin, X., and B. Luke (2006). Comparison of three surface wave measurements and a seismic downhole measurement in a complex-layered system, in *Site and Geomaterial Characterization*, A. Puppala, D. Fratta, K. Alshibli, and S. Pamukcu (Editors), American Society of Civil Engineers, Reston, Virginia, 212–219.
- Konno, K., and T. Ohmachi (1998). Ground-motion characteristics estimated from spectral ratio between horizontal and vertical components of microtremor, *Bull. Seismol. Soc. Am.* **88**, no. 1, 228–241.
- Lermo, J., and F. J. Chávez-García (1994). Are microtremors useful in site response evaluation? *Bull. Seismol. Soc. Am.* **84**, no. 5, 1350–1364.
- Leyton, F., A. Leopold, G. Hurtado, C. Pastén, S. Ruiz, G. Montalva, and E. Saéz (2018). Geophysical characterization of the Chilean seismological stations: First results, *Seismol. Res. Lett.* **89**, no. 2A, 519–525.
- Luke, B., and C. Calderón-Macías (2007). Inversion of seismic surface wave data to resolve complex profiles, *J. Geotech. Geoenviron. Eng.* **133**, no. 2, 155–165.
- Murvosh, H., B. Luke, and C. Calderón-Macías (2013). Shallow-to-deep shear wave velocity profiling by surface waves in complex ground for enhanced seismic microzonation of Las Vegas, Nevada, *Soil Dynam. Earthq. Eng.* **44**, 168–182.

- Oubaiche, E. H., J. L. Chatelain, M. Hellel, M. Wathelet, D. Machane, R. Bensalem, and A. Bouguern (2016). The relationship between ambient vibration H/V and SH transfer function: Some experimental results, *Seismol. Res. Lett.* **87**, no. 5, 1112–1119.
- Oztoprak, S., and M. D. Bolton (2013). Stiffness of sands through a laboratory test database, *Géotechnique* **63**, no. 1, 54.
- Pastén, C., M. Sáez, S. Ruiz, F. Leyton, J. Salomón, and P. Poli (2016). Deep characterization of the Santiago basin using HVSR and cross-correlation of ambient seismic noise, *Eng. Geol.* **201**, 57–66.
- Renalier, F., D. Jongmans, A. Savvaidis, M. Wathelet, B. Endrun, and C. Cornou (2010). Influence of parameterization on inversion of surface wave dispersion curves and definition of an inversion strategy for sites with a strong V-S contrast, *Geophysics* **75**, no. 6, B197–B209.
- Rubinstein, J. L., and G. C. Beroza (2004). Evidence for widespread nonlinear strong ground motion in the  $M_w$  6.9 Loma Prieta earthquake, *Bull. Seismol. Soc. Am.* **94**, no. 5, 1595–1608.
- Ruiz, S., R. Madariaga, M. Astroza, G. R. Saragoni, M. Lancieri, C. Vigny, and J. Campos (2012). Short-period rupture process of the 2010  $M_w$  8.8 Maule earthquake in Chile, *Earthq. Spectra* **28**, no. S1, S1–S18.
- Sawazaki, K., H. Sato, H. Nakahara, and T. Nishimura (2009). Time-lapse changes of seismic velocity in the shallow ground caused by strong ground motion shock of the 2000 Western-Tottori earthquake, Japan, as revealed from coda deconvolution analysis, *Bull. Seismol. Soc. Am.* **99**, no. 1, 352–366.
- Scherbaum, F., K.-G. Hinzen, and M. Ohrnberger (2003). Determination of shallow shear wave velocity profiles in the Cologne, Germany area using ambient vibrations, *Geophys. J. Int.* **152**, no. 3, 597–612.
- Schnabel, P. B., J. Lysmer, and H. B. Seed (1972). SHAKE: A computer program for earthquake response analysis of horizontally layered sites, *Rept. No. UCB/EERC-72/12*, Earthquake Engineering Research Center, University of California, Berkeley, California, 102 pp.
- Seed, H. B., and I. M. Idris (1970). Soil moduli and damping factors for dynamic response analysis, *Technical Report EERC-70-10*, University of California, Berkeley.
- Seed, H. B., R. T. Wong, I. M. Idriss, and K. Tokimatsu (1986). Moduli and damping factors for dynamic analyses of cohesionless soils, *J. Geotech. Eng.* **112**, no. 11, 1016–1032.
- Shen, C., Y. Xu, Y. Pan, A. Wang, and L. Gao (2016). Sensitivities of phase-velocity dispersion curves of surface waves due to high-velocity-layer and low-velocity-layer models, *J. Appl. Geophys.* **135**, 367–374.
- Steidl, J. H., A. G. Tumarkin, and R. J. Archuleta (1996). What is a reference site? *Bull. Seismol. Soc. Am.* **86**, no. 6, 1733–1748.
- Sun, J. I., R. Golesorkhi, and H. B. Seed (1988). *Dynamic Moduli and Damping Ratios for Cohesive Soils*, Earthquake Engineering Research Center, University of California Berkeley.
- Thompson, E. M., L. G. Baise, R. E. Kayen, and B. B. Guzina (2009). Impediments to predicting site response: Seismic property estimation and modeling simplifications, *Bull. Seismol. Soc. Am.* **99**, no. 5, 2927–2949.
- Verdugo, R. (2009). Amplification phenomena observed in downhole array records generated on a subductive environment, *Phys. Earth Planet. In.* **175**, nos. 1/2, 63–77.
- Wathelet, M. (2008). An improved neighborhood algorithm: Parameter conditions and dynamic scaling, *Geophys. Res. Lett.* **35**, no. 9, doi: [10.1029/2008GL033256](https://doi.org/10.1029/2008GL033256).
- Wathelet, M., D. Jongmans, and M. Ohrnberger (2004). Surface-wave inversion using a direct search algorithm and its application to ambient vibration measurements, *Near Surf. Geophys.* **2**, no. 4, 211–221.
- Xia, J., R. D. Miller, C. B. Park, J. A. Hunter, J. B. Harris, and J. Ivanov (2002). Comparing shear-wave velocity profiles inverted from multi-channel surface wave with borehole measurements, *Soil Dynam. Earthq. Eng.* **22**, no. 3, 181–190.
- Zeghal, M., A. W. Elgamal, H. T. Tang, and J. C. Stepp (1995). Lotung downhole array. II: Evaluation of soil nonlinear properties, *J. Geotech. Eng.* **121**, no. 4, 363–378.

Department of Geophysics  
University of Chile  
Blanco Encalada 2002  
Santiago 8370449  
Chile  
msaez@dgf.uchile.cl  
sruiz@dgf.uchile.cl  
(M.S., S.R.)

Department of Civil Engineering  
University of Chile  
Blanco Encalada 2002  
Santiago 8370449  
Chile  
cpasten@ing.uchile.cl  
(C.P., J.S.)

Manuscript received 21 September 2017;  
Published Online 10 July 2018